**53rd AIAA/ASME/ASCE/AHS/ASC Structures, Structural Dynamics and Materials Conference
20th AI**
23 - 26 April 2012, Honolulu, Hawaii

AIAA 2012-1512

Piezoelectric Morphing versus Servo-Actuated MAV Control Surfaces

Osgar John Ohanian III[*], Christopher Hickling[†], Brandon Stiltner[‡], Etan D. Karni[§],
AVID LLC, Blacksburg, VA, 24060,

Kevin B. Kochersberger[**], Troy Probst[††]
Virginia Polytechnic Institute and State University, Blacksburg, VA, 24060

Paul A. Gelhausen[‡‡]
AVID LLC, Yorktown, VA, 23692

and

Aaron P. Blain[§§]
Air Force Research Laboratory, Munitions Directorate, Eglin AFB, FL, 32542

A novel morphing control surface design employing piezoelectric Macro Fiber Composite (MFC) actuators is compared to a servo-actuated system. The comprehensive comparison including aerodynamics, size, weight, power, bandwidth, and reliability has revealed several observations. The conformal morphing airfoil geometry increases the lift-to-drag ratio over a servo-actuated flapped airfoil design, showing benefits in aerodynamic efficiency. The embedded MFC actuators eliminate the servo actuator volume from vehicle packaging; however, the MFC drive electronics must be taken into consideration. While the weight of the current prototype morphing system exceeds that of a traditional servo and linkage implementation, the weight is comparable and may not be prohibitive for some applications. The comparable power requirement and superior bandwidth make the morphing actuation a feasible and attractive approach for certain air vehicle designs. An order of magnitude increase in bandwidth was observed using the morphing flight control actuation. Ongoing reliability testing of the morphing specimens has demonstrated that solid-state morphing actuation has not failed within 10^5 cycles. Flight tests are planned to fully prove the benefits of the morphing actuation over a servo-actuated design.

Nomenclature

A	=	Airfoil planform area, ft^2
C_d	=	Drag coefficient (2D), $D/(0.5\rho V^2 A)$
C_l	=	Lift coefficient (2D), $L/(0.5\rho V^2 A)$
D	=	Drag, lb
L	=	Lift, lb
α	=	Angle of Attack, degrees
β	=	Airfoil support angle, degrees
ρ	=	Air density, slug/ft^3

DISTRIBUTION A. Approved for public release, distribution unlimited. (96ABW-2011)

---

[*] Director of Technology Development, AVID LLC, Blacksburg, VA, AIAA Member.
[†] Aerospace Engineer, AVID LLC, Blacksburg, VA.
[‡] Aerospace Engineer, AVID LLC, Blacksburg, VA, AIAA Member.
[§] Aerospace Engineer, AVID LLC, Blacksburg, VA, AIAA Member.
[**] Research Associate Professor, Mechanical Engineering, Virginia Tech, Blacksburg, VA, AIAA Associate Fellow.
[††] Graduate Research Assistant, Mechanical Engineering, Virginia Tech, Blacksburg, VA, AIAA Student Member.
[‡‡] CTO, AVID LLC, Yorktown, VA, AIAA Senior Member.
[§§] 1st Lieutenant, Air Force Research Laboratory, Eglin AFB, FL.

1

Report Documentation Page

Public reporting burden for the collection of information is estimated to average 1 hour per response, including the time for reviewing instructions, searching existing data sources, gathering and maintaining the data needed, and completing and reviewing the collection of information. Send comments regarding this burden estimate or any other aspect of this collection of information, including suggestions for reducing this burden, to Washington Headquarters Services, Directorate for Information Operations and Reports, 1215 Jefferson Davis Highway, Suite 1204, Arlington VA 22202-4302. Respondents should be aware that notwithstanding any other provision of law, no person shall be subject to a penalty for failing to comply with a collection of information if it does not display a currently valid OMB control number.

1. REPORT DATE	2. REPORT TYPE	3. DATES COVERED
APR 2012		**00-00-2012 to 00-00-2012**

4. TITLE AND SUBTITLE	5a. CONTRACT NUMBER
Piezoelectric Morphing versus Servo-Actuated MAV Control Surfaces	5b. GRANT NUMBER
	5c. PROGRAM ELEMENT NUMBER
6. AUTHOR(S)	5d. PROJECT NUMBER
	5e. TASK NUMBER
	5f. WORK UNIT NUMBER
7. PERFORMING ORGANIZATION NAME(S) AND ADDRESS(ES) **Virginia Polytechnic Institute and State University,Blacksburg,VA,24060**	8. PERFORMING ORGANIZATION REPORT NUMBER
9. SPONSORING/MONITORING AGENCY NAME(S) AND ADDRESS(ES)	10. SPONSOR/MONITOR'S ACRONYM(S)
	11. SPONSOR/MONITOR'S REPORT NUMBER(S)

12. DISTRIBUTION/AVAILABILITY STATEMENT
Approved for public release; distribution unlimited

13. SUPPLEMENTARY NOTES
Presented at the 53rd AIAA/ASME/ASCE/AHS/ASC Structures, Structural Dynamics and Materials Conference, 23 - 26 April 2012, Honolulu, Hawaii, Government or Federal Purpose Rights License, 1/20

14. ABSTRACT
A novel morphing control surface design employing piezoelectric Macro Fiber Composite (MFC) actuators is compared to a servo-actuated system. The comprehensive comparison including aerodynamics, size, weight, power, bandwidth, and reliability has revealed several observations. The conformal morphing airfoil geometry increases the lift-to-drag ratio over a servo-actuated flapped airfoil design, showing benefits in aerodynamic efficiency. The embedded MFC actuators eliminate the servo actuator volume from vehicle packaging however, the MFC drive electronics must be taken into consideration. While the weight of the current prototype morphing system exceeds that of a traditional servo and linkage implementation, the weight is comparable and may not be prohibitive for some applications. The comparable power requirement and superior bandwidth make the morphing actuation a feasible and attractive approach for certain air vehicle designs. An order of magnitude increase in bandwidth was observed using the morphing flight control actuation. Ongoing reliability testing of the morphing specimens has demonstrated that solid-state morphing actuation has not failed within 105 cycles. Flight tests are planned to fully prove the benefits of the morphing actuation over a servo-actuated design

15. SUBJECT TERMS

16. SECURITY CLASSIFICATION OF:			17. LIMITATION OF ABSTRACT	18. NUMBER OF PAGES	19a. NAME OF RESPONSIBLE PERSON
a. REPORT **unclassified**	b. ABSTRACT **unclassified**	c. THIS PAGE **unclassified**	**Same as Report (SAR)**	**19**	

I. Introduction

As the need for operations in urban canyon environments increases, there is a similar push to miniaturize the air platforms performing missions in these situations. The research described herein attempts to address both of these important areas. Attaining flight control actuation that can achieve the maneuverability requirements to navigate tight city streets is quite a challenge in itself, but approaches that can scale to miniature sizes while maintaining high reliability, low weight and low packaging volume are even more impressive. The motivation behind this current effort was to develop smart material morphing flight control actuation that will simultaneously increase performance and reduce the size, weight, and power (SWaP) impacts to the air platform.

There are many small and micro air vehicles (MAVs) that are in service today. Most of these use some kind of small servomotor as an actuator in the flight control system. These conventional systems work well, and have leveraged the advances in model aircraft electronics over the past several decades. Servos are quite lightweight and have acceptable power consumption, but occupy significant volume, and are less reliable than desired. On small vehicles operating at low Reynolds numbers, flow separation over conventional flap or aileron surfaces is responsible for large portions of the overall vehicle drag.

A conformal smart material actuator has the potential to address several of the disadvantages of the servo-mechanical devices. Since the actuator has no moving parts that can be worn or contaminated, the reliability is likely an order of magnitude better. The actuator is integral with the skin, so the volume of the actuator is negligible. With a reduced number of moving parts, the robustness during assembly and deployment will be much better for a smart material wing. The power and control electronics can be placed somewhat independently of the actuators, which improves the ability to strategically locate the volume and weight. The continuous mold-line curvature of the actuator is ideal for low Reynolds number applications, and eliminates the drag due to separation at the hinge line and drag of linkage hardware that is evident on so many small and micro UAVs.

A solid-state morphing control surface is a promising solution to the challenging problem outlined above. By 'solid-state', it is implied that there are no servos, linkages, or moving parts other than the conformal shape change of the aerodynamic surfaces. Instead, smart materials are used to implement the morphing capability; specifically piezoelectric Macro Fiber Composites (MFC) are used [1][2], shown in Figure 1. MFCs are primarily capacitive devices (typically 0.42 nF per cm2), with an operating voltage range from -500V to +1500V. While instantaneous current requirements can be significantly higher than the average value, currents for low-rate actuation are typically on the order of single milliamps. MFCs are environmentally sealed, flexible, and damage tolerant.
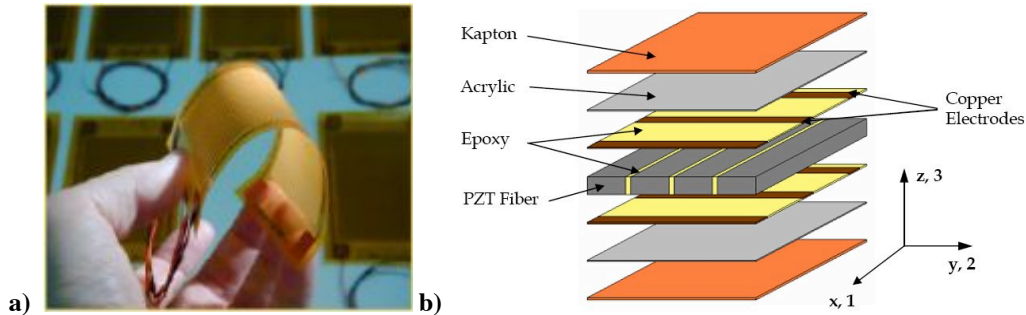

Figure 1. Macro Fiber Composite (MFC): a) Flexible nature of MFC b) Exploded view of construction [1].

The bimorph concept, shown on the left in Figure 2, can convert the axial strain of the piezoelectric fibers into an overall bending motion of an aircraft skin. The implementation of this smart material bimorph in a morphing airfoil cross section is depicted schematically in Figure 2 on the right. The upper surface of the airfoil is controlled through MFC bending, while the bottom "wiper" surface passively slides along with the upper surface to complete the airfoil cross-section. The MFC bimorph allows for camber deflection in either direction, and the piezoelectric material has the potential for exceptional bandwidth; both are beneficial characteristic for closed loop flight control.
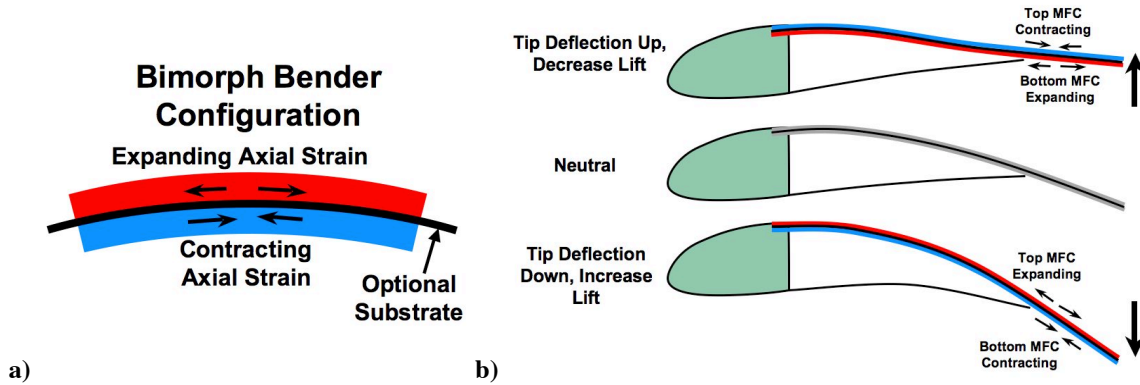
Figure 2. Smart material actuation: a) Bimorph configuration, b) Morphing airfoil employing a single bimorph.

This morphing technology was applied to the wing and tail of a generic micro air vehicle created by the Air Force Research Laboratory (AFRL) as a research platform, the GENMAV [3]. The basic airframe design and fabricated test article are shown in Figure 3, and further modifications to the airframe for exploratory research are documented in reference [4].
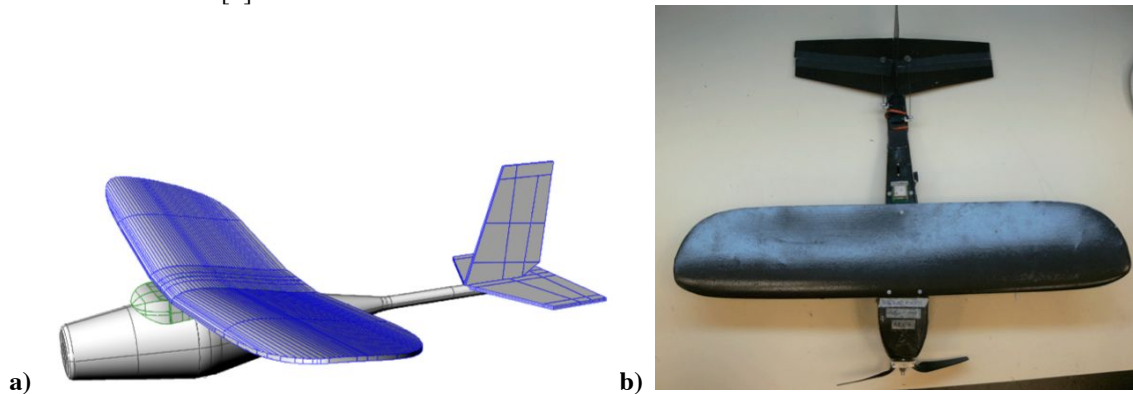

Figure 3. AFRL generic platform for MAV research, GENMAV: a) Conceptual design [3], b) Flight test airframe [4].

This generic platform was chosen because it enables a fair comparison of the new morphing actuation to a traditional servo-actuated version, while focusing on the technology and not the airframe design. Component testing, wind tunnel testing, and flight-testing will be used to fully assess the advantages and disadvantages of conformal morphing and servomotor actuation on this platform. The following sections of the paper describe: a review of existing work, design of the morphing control surfaces, experimental setup, experimental results and discussion, and the conclusions.

II. Literature Review

The increased interest in small air vehicle research has resulted in several new research initiatives aimed at improving the performance of these vehicles in the low Reynolds number regime [5][6][7][8]. One of the more significant demonstrations of the application of morphing technology to agile maneuvering is found in [9], where servo-actuated rods were used to twist the wing of a 28" span aircraft. In these demonstrations, roll rates of up to 800 deg/sec were achieved, but a noticeable degradation in the L/D was observed as asymmetric drag increased with wing deflection. In the case of small, low powered aircraft, maneuvering drag can be significant in the overall performance and should be considered when designing for a given roll rate.

Aside from conventional servo-actuated controls, recent adaptive air vehicle design has focused on control of wing twist by wing warping [10], or variable planform geometry either through sweep or wing folding [11]. Bilgen et al. [12][13] have shown the effectiveness of conformal actuators in providing roll control for a 0.76 m wingspan aircraft through asymmetric camber control. Additionally, active flow control has been shown to increase lift and reduce drag by affecting the boundary layer; particularly important in low Reynolds number flows. Lee, et al. [14]

have demonstrated boundary layer control using synthetic jets, and Ghee and Leishman [15] have shown similar results using periodic jet blowing. Pern et al. [16] have demonstrated flow control by pulsing the upper surface of an airfoil with a PZT actuator, resulting in a crossflow-induced vortex that reduces drag and increases lift.

Gern et al. [17] performed research to study the performance of traditional flaps versus airfoil morphing. Via simulation, they claim that a morphing trailing edge wing can produce up to 50% more rolling moment than a conventional flapped wing. They also claim that the absence of sharp edges and deflected surfaces reduces the radar signature of the vehicle. Researchers have also shown that variable camber flaps can reduce the required actuation energy as opposed to conventional flapped wings. In [18], Marques et al. experimentally achieve a 40% decrease in actuation energy required. Other notable research efforts in the area of morphing wings and morphing airfoils can be found in [19][20][21][22][23].

Specific research into using Macro Fiber Composite actuators in MAV applications was pioneered by Bilgen et al. [12][13][24][25]. Ohanian et al. continued to investigate MFC morphing actuation with the intent to minimize the size, weight and power (SWaP) impact in [26]. Probst et al. [27] investigated the 2-D aerodynamics of MFC morphing airfoils and the control response of such designs. This present work is a continuation of the research in MFC morphing actuation in [26] and [27], attempting to provide a multidisciplinary, quantitative comparison between morphing flight control actuation and industry-standard servomotor actuation.

III.   Morphing Control Surface Design

The use of embedded piezoelectric fiber actuators in aircraft skins enables a shape changing capability without external actuators, linkages, and kinematics. The "smart material" coupling between the electric and mechanical domains requires only a voltage potential to attain the desired mechanical deflection. The simplicity of the concept is attractive, but care must be taken to ensure a structure that is flexible enough to morph effectively and strong enough to carry the necessary aerodynamic loads. The design of the morphing control surfaces, the control thereof, and the air vehicle platform for performance comparisons will be described in the following subsections.

A. Morphing Wing and Tail

One of the fundamental tasks for this technology's development is the design and analysis of the morphing airfoil mechanism. From an aerodynamic perspective there are two main components contributing: the performance of the selected airfoil design while un-deflected, and the effects that are imparted by the morphing deflections. The amplitude of the morphing and the percentage of the structure that morphs both play a role in the final performance of the actuation approach.

The wing airfoil selection process began with a survey of existing airfoils listed in the UIUC Airfoil Database [24]. Initial candidate airfoils were selected based on quoted low Reynolds usage, as the vehicle to be designed will likely operate in the range of 50,000 to 200,000. The Selig S1210 was ultimately selected as the baseline wing airfoil, on the basis of its high maximum lift coefficient, a relatively good maximum L/D, and a thin aft cross section that was favorable for MFC integration. This airfoil was used as a starting point for adaptation and incorporation of morphing actuation.

The morphing section of the wing planform, an outboard aileron, has a modified structure to allow for maximum morphing deflection. A foam core with composite shell is used to construct a rigid D-box (outside skin combined with internal shearweb). Materials such as fiberglass, carbon, or Kevlar could be used as the composite skin in this design. The D-box structure covers the leading 20% of the airfoil cross-section. This serves as a rigid mounting surface for the morphing skin with MFC bimorphs, which represents the upper surface of the airfoil outline. A flexible composite 'wiper' surface completes the lower airfoil surface. The wiper is only connected to the D-box and slides along the upper morphing skin as it deflects. The wiper is molded to produce an upward pre-stress, such that when the morphing skin deflects upward the wiper will track it, keeping a closed airfoil cross section. The aft section of the airfoil is hollow to allow maximum morphing actuation. A cross section view of this portion of the wing is shown in Figure 4. The prototype wings showing the morphing and servo-actuated control surface concepts are shown in Figure 5.
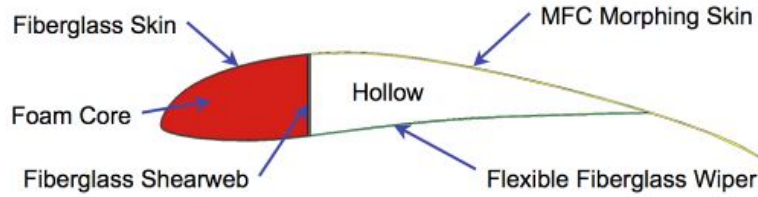
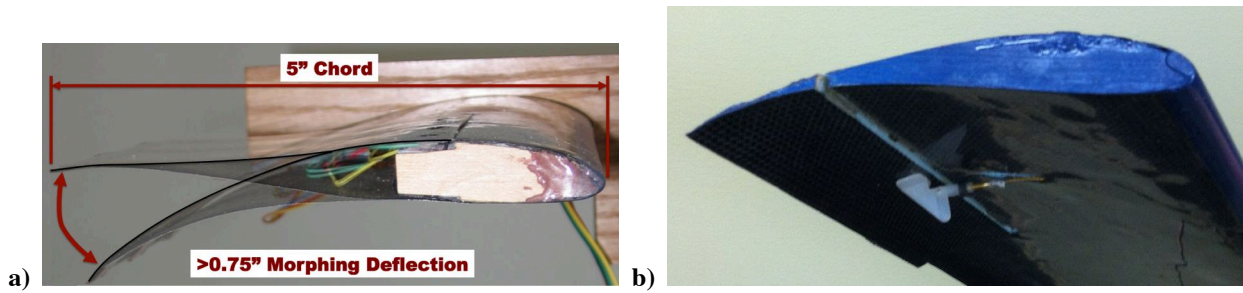**Figure 4. Morphing airfoil structural cross section.**

Figure 5. Prototypes of morphing and servo-driven airfoils: a) Morphing airfoil with embedded MFC actuators, b) 30%-chord flapped airfoil with servo-linkage actuation.

This morphing approach has been successfully applied to a high-lift wing airfoil with a thickness of roughly 12%. However, the technique can also be applied to composite thin plate structures such as a cambered wing or tail surface. The tail surfaces of the GENMAV airframe already incorporated a simple thin plate construction for the horizontal and vertical tails. This gave the opportunity to illustrate the versatility of the morphing technology to be adapted to many aerodynamic applications, by demonstrating morphing thin and thick airfoil designs.

The thin plate GENMAV horizontal tail surface was modified to incorporate two embedded MFC bimorphs to enable morphing deflections. The structure of the skin was modified to provide stiffness in critical areas, while adding flexibility for morphing. Specifically, span-wise stiffness was increased by using uni-directional carbon fiber at the leading and trailing edge, while the main skin of the tail is a compliant layup of composite layers allowing for maximum morphing deflection. The stiffness of the structure also determines the maximum actuation frequency, since the natural frequency of the first bending mode is a practical limit for mechanical control of the structure. These considerations resulted in the tail design shown in Figure 6.
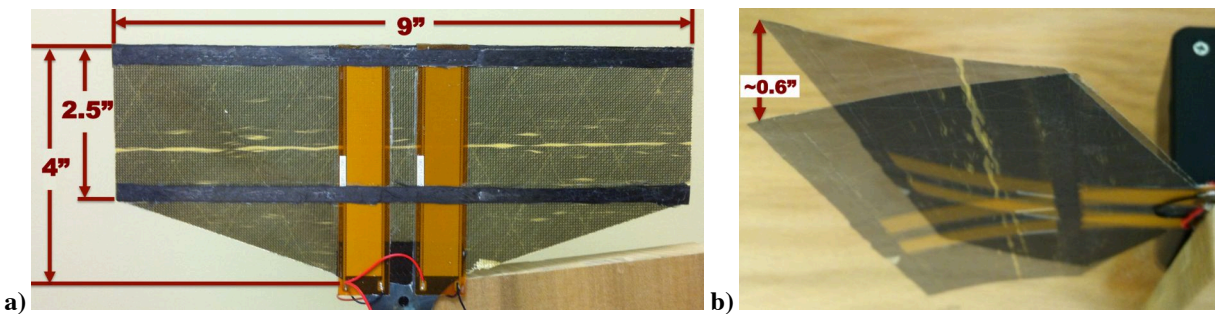

Figure 6. Morphing horizontal tail: a) MFC layout on carbon fiber and Kevlar layup, b) Morphing deflection of elevator.

B. Control of Actuator Deflection

Piezoelectric actuators typically exhibit the nonlinear phenomenon of hysteresis and creep. Hysteresis implies that the deflection state of the morphing control surface is affected by its previous history. The creep phenomenon causes the actuator deflection to change slowly over long timescales. If uncompensated, these nonlinearities could degrade flight control performance. The key for micro air vehicle integration is to find a solution that sufficiently addresses these concerns, while not incurring a large weight or complexity penalty. The authors have identified

several approaches to address this: closed-loop control at the vehicle level (MFCs uncompensated); open-loop compensation for MFC nonlinearities; and closed-loop control of MFC deflection.

The first approach assumes that the inertial sensor feedback at the vehicle level will be sufficient to control the vehicle's flight using the nonlinear actuators. This would require integral control on the vehicle steady state error to account for the effects of hysteresis and creep. This is the lightest weight and simplest solution, but the performance would need to be verified before this was chosen for a final design.

The next potential solution involves compensating for the MFC nonlinearities through open-loop control. Open-loop control produces the desired system output by modifying the system input using predetermined models of the system. This approach eliminates the need for a sensor, but requires a highly accurate model of the system. If the actual system experiences unexpected disturbances or deviates from the predetermined model, the open-loop control will not account for this variability as a closed-loop system would. The most attractive aspect of this approach is that it could be performed entirely in software and may not require any additional hardware or increased vehicle weight.

The final option, and most robust of the three, is to attain a feedback signal on the position of the MFC and use closed-loop control algorithms to accurately deflect the actuator. Closed-loop control has proven to be effective at removing creep and eliminating the effect of hysteresis. Closed-loop control uses feedback to determine the state of the system and modifies the system input based on this feedback. This type of system is preferred for its ability to handle changes, disturbances, errors, and variability in the system. However, this approach requires system feedback that involves integrating a sensor into the wing and/or tail and increasing overall system weight. The most difficult hurdle in this approach is generating the sensor signal that represents MFC position.

In either of the open-loop or closed-loop approaches, it would be beneficial to remove the effects of hysteresis. An inverse hysteresis operator (IHOp) has been developed from a reduced-order model of the hysteretic behavior to accomplish this. The details of these developments may be referenced in [27]. A plot of the experimental hysteresis deflections and model fit are shown in Figure 7, as well as the linearization of a morphing actuator using the hysteresis inversion.
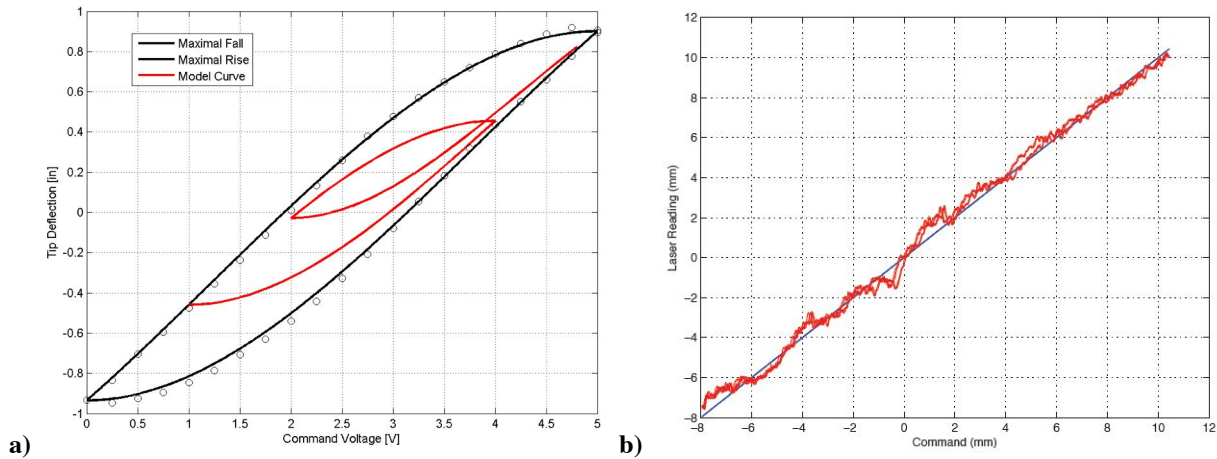

Figure 7. Hysteresis nonlinearity: a) Example of MFC bimorph hysteresis loop, b) Inversion of hysteresis nonlinearity resulting in near linear output.

C. Platform for Comparison with Servo Actuation

The GENMAV airframe was modified to incorporate morphing ailerons and a morphing elevator. The vertical tail was left un-actuated, as designed in the original GENMAV, to provide passive lateral stability. Morphing actuation could be added to this surface as well, but was omitted to minimize weight and demonstrate successful flight control using two input channels. A preliminarily assembled flight vehicle of the morphing GENMAV airframe is shown in Figure 8 (only morphing ailerons installed).
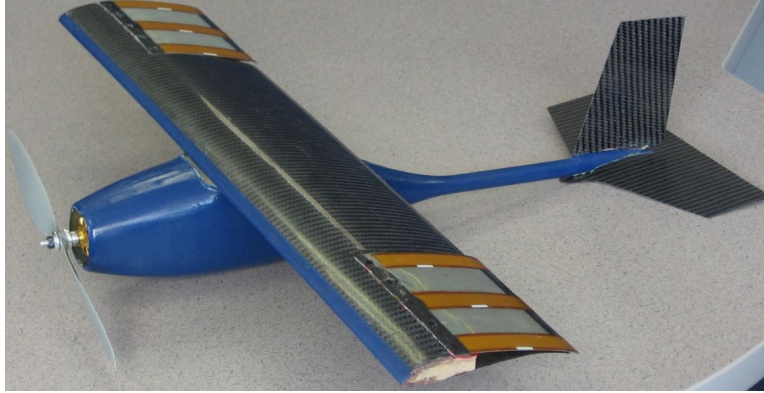
Figure 8. Modified GENMAV with morphing actuation for comparison to servo-actuated flight control.

IV.   Experimental Setup and Procedure

1. Bench Top Experimental Setup

Several morphing tests were performed in a bench top laboratory setting, while other tests were performed in a 2-dimensional wind tunnel. Figure 9 shows the setup for morphing deflection bench tests that supported deflection tests, hysteresis/creep modeling, step response tests, and frequency response tests.   In this setup, the laser displacement sensor (MTI Microtrak II-SA 300-200) measurement, combined with the National Instruments data acquisition unit, is the main source of data. High voltage control signals were provided to the MFC elements using a custom-made circuit board developed in collaboration with AM Power Systems. The micro servo selected for comparison was the Futaba S3156MG metal gear micro servo. For servo actuation a pulse width modulated (PWM) signal was generated to drive the servo. For power measurements, a current sensing shunt resistor was used on the power line to the servo actuator or high voltage supply to the MFC, and the 20 kHz signal was integrated over time and multiplied by voltage to calculate power. The high sample rate was necessary to capture the rising and falling edge of the digital servo power waveform. For hysteresis tests, a custom LabView program was used to command ramping input to the morphing structure, while for frequency response tests supplied a set of sine wave inputs to the system of various frequencies spanning the bandwidth range.
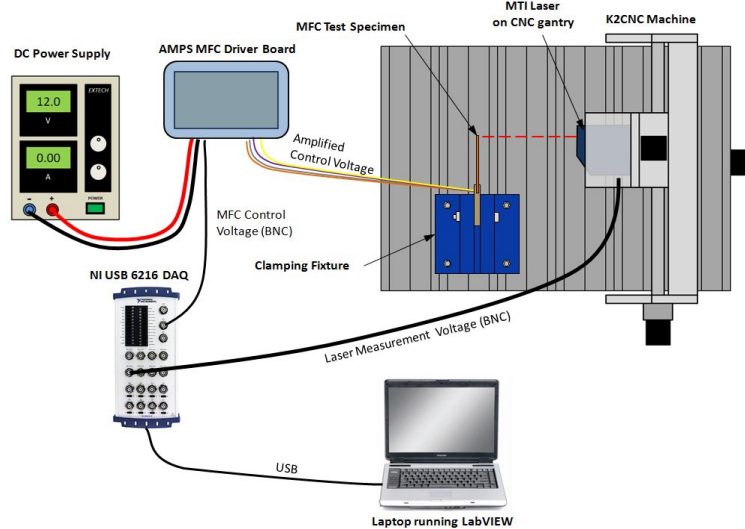

Figure 9. Bench test setup for morphing deflection measurement.

2. Wind Tunnel Experimental Setup

The 2D aerodynamic characteristics of the morphing and servo-actuated airfoils were evaluated in the low-speed wind tunnel located in Virginia Tech's Center for Intelligent Material Systems and Structures (CIMSS). Previous morphing airfoil tests in this tunnel are documented in [24]. As Bilgen [30] describes, the wind tunnel is a small,

American Institute of Aeronautics and Astronautics

open-circuit tunnel with a 136 mm tall and 356 mm wide cross section. The test section is constructed from acrylic and has several ports for the placement of Pitot-static probes and other measurement sensors. The tunnel includes two fans which can generate wind velocities between 2 and 22 m/s. Detailed wind tunnel specifications can be found in [30]. The wind tunnel test setup is shown in Figure 10, with one of the morphing airfoil test specimens from this research effort shown installed in the wind tunnel test section.
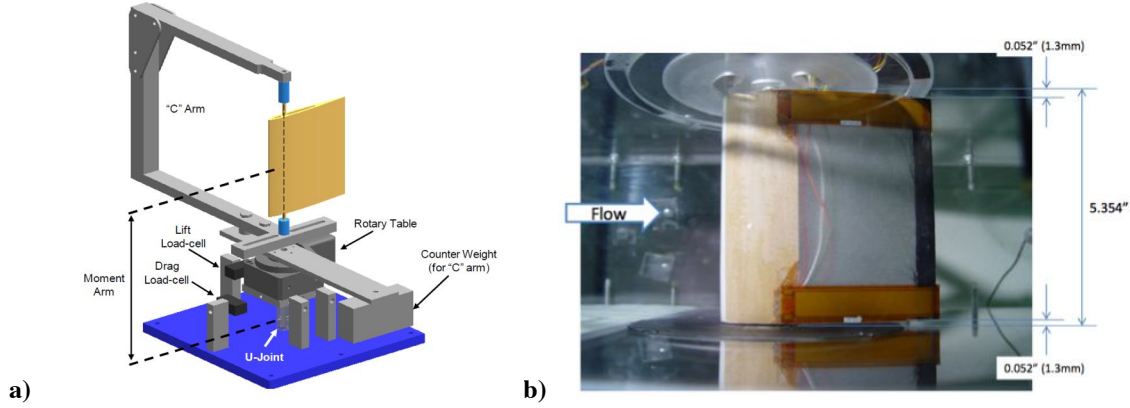

Figure 10. Morphing airfoil with two integrated MFC 85mm x 14mm bimorphs installed in 2D wind tunnel: a) CAD model of the balance support system [30], b) Top view of airfoil (side view of tunnel).

One important variable, which will be used throughout the wind tunnel section of the paper, is the airfoil "support angle", β. Here the support angle is defined as the angle between the free stream wind velocity and the airfoil chord line at zero actuation and no loading. This angle, shown in Figure 11, is constant at all levels of airfoil control surface actuation and is solely controlled by the rotation of the airfoil and C-arm assembly on the rotary table.
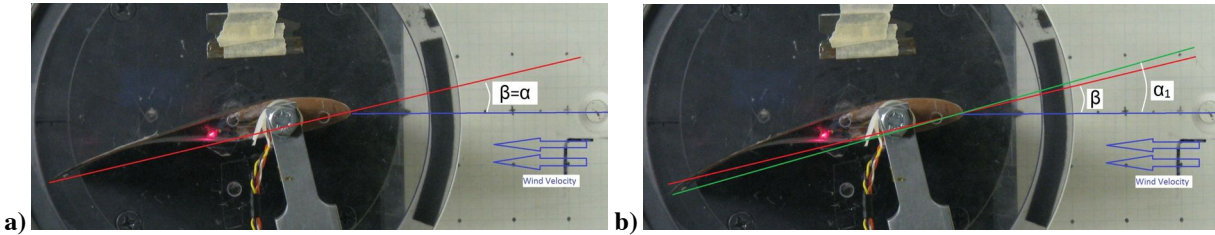

Figure 11. Definition of airfoil "support angle" in 2D wind tunnel tests.

At zero actuation, the support angle is equivalent to the true angle of attack, α. The angle of attack is defined as the angle between the free stream velocity and the chord line, which is defined by the leading edge and trailing edge points. However, as the control surface actuates, the angle of attack changes as the trailing edge deflects up and down due to morphing. The support angle allows for simpler comparisons between different angles to the flow without the additional complication of a changing angle of attack. Most figures in this paper use support angle as an independent variable.

V.   Experimental Results

A wide variety of disciplines were evaluated to compare the morphing control surface actuation to traditional servomotor actuation. Analysis and experimental data are used to demonstrate the advantages and disadvantages of each approach for MAV control. The areas addressed include: 2D aerodynamics, size, weight, power, bandwidth, and reliability.

A. Airfoil Aerodynamics

A combination of analysis and wind tunnel experiments were used to assess the aerodynamic benefits of morphing actuation. Initial aerodynamic analysis was performed in XFOIL [29]. These initial analyses were followed up with 2-dimensional wind tunnel tests. Initial tests were performed with morphing actuation sweeps and

servo-actuated flap deflection sweeps. Discrepancies in fabrication between the morphing and servo-actuated airfoils made the drag measurements uncertain and difficult to compare. To address this issue, the measured shape of each deflected airfoil was rapid prototyped in a single solid airfoil with uniform surface finish properties for both airfoils. The following subsections describe the results.

3. Morphing Actuation Tests

Initial wind tunnel tests explored the effects of control surface deflection (morphing), angle of attack, and freestream velocity. The airfoil in the tests presented incorporated two 85mm x 14mm MFC bimorphs. Probst et al. describe these experimental results in [27], but a summary will be included here for completeness. The lift and drag data from wind tunnel tests at 13 m/s and Reynolds number of 107,900 are presented in Figure 12.
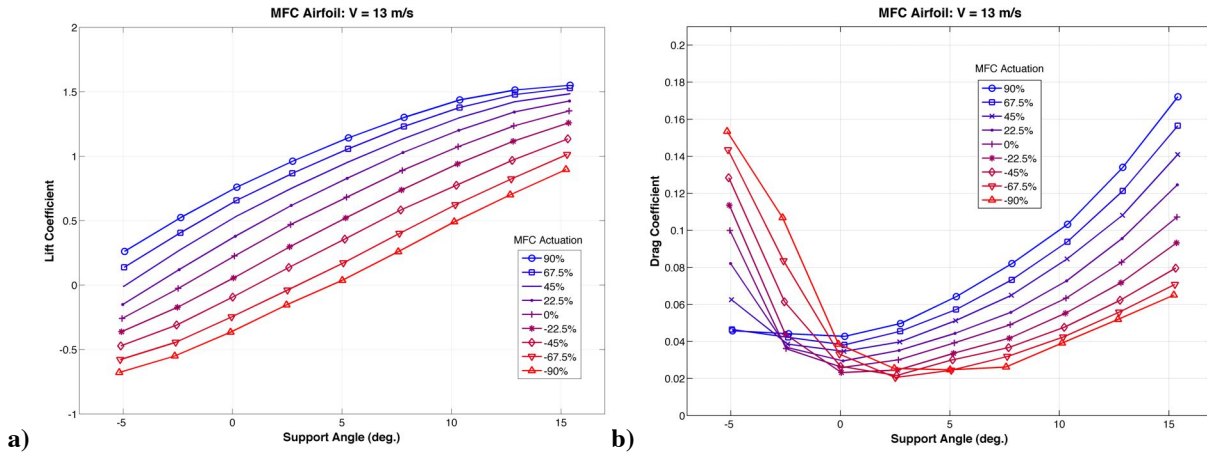

Figure 12. Morphing actuation effects on lift vs. airfoil support angle.

As can be seen in Figure 12, the variation in lift coefficient due to morphing actuation is significant. The difference between the maximum (90% actuation) and minimum (-90% actuation) lift coefficient is roughly 1.1 over a large range of airfoil support angles. As stall ensues above 10° for the highest actuation levels (in 2-D flow), the control authority starts to diminish, with a change of 0.65 in lift coefficient at 15° angle of attack. The maximum lift coefficient observed was 1.55 at maximum positive actuation and angle, while the minimum lift coefficient was -0.68 for negative actuation at the minimum angle of airfoil rotation.

Looking at drag characteristics, it can be seen that the support angle of minimum drag decreases as the actuation percentage increases. For positive support angles, drag increases with increasing morphing actuation and lift generation, while for negative actuation drag decreased with increasing actuation. The coefficient of drag for 0% actuation ranges from 0.047 at a support angle of -5° to 0.107 at a support angle of 15°. The minimum coefficient of drag measured is 0.027 at 0° support angle.

The measured drag values are larger than expected for this airfoil that is adapted from the Selig S1210 design (0.031 for Re 101,100 at angle of attack of 5° [28] compared to 0.039 at angle of attack of 5° in present tests for un-deflected case). Some of the added drag contribution can be attributed to the tunnel itself. The approximately 1.5mm gap between the airfoil section and the tunnel wall exposes the pin supports, resulting in drag from the gap and pins. The drag from the pins alone has been shown to be as high as $C_D = 0.018$ [25]. Higher turbulence levels in the tunnel also increase measured drag. Finally, the airfoil surface itself is not smooth due to MFC installation and airfoil fabrication. When comparing test data between morphing and servo-actuated airfoil geometries, the drag measurements were inconclusive. This was attributed to discrepancies in fabrication between the two airfoils. To better assess the aerodynamic comparison between morphed and flapped geometry, airfoils with identical fabrication techniques and surface finish were needed.

4. Morphing vs. Flapped Airfoils

The goal of this subsequent test was to quantify the differences between a continuous airfoil, such as that achieved by an MFC actuated airfoil, and a discontinuous flapped airfoil. Specifically, the coefficients of lift and drag and the lift-to-drag ratio (L/D) were the parameters of interest. Due to the low Reynolds number of the flow, these aerodynamic characteristics are highly dependent on the surface finish and profile of the airfoils. In order to isolate the effects of continuous versus discontinuous geometry, the airfoils were modeled in CAD at maximum

actuation observed, and rapid prototyped with the same surface finish and leading edge geometry. The servo airfoil was based on a CAD model of a flapped airfoil with 30% chord flaps deflected 20 degrees, with the trailing edge deflection being comparable to the morphed trailing edge deflection. The Reynolds number for these wind tunnel tests was calculated as 105,573 for the flow speed tested. Except for the differences between continuous or discontinuous aft geometries, the two airfoils models were identical. Both had 5" chord and 5.25" span. The trailing edge deflections of each also matched very well within a few hundredths of a degree. The CAD model profiles are shown in Figure 13.
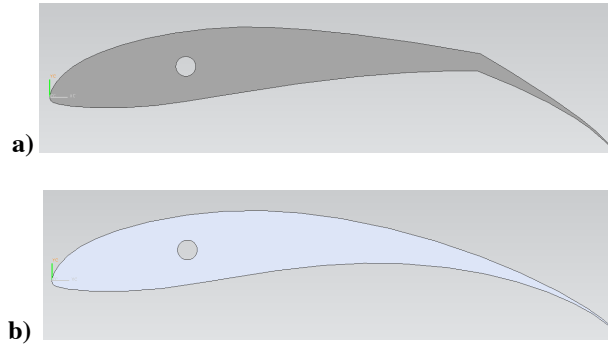

Figure 13. CAD profiles of rapid prototyped airfoils: a) flapped and b) continuous airfoils.

After modeling, the parts were sent to Virginia Tech's Mechanical Engineering machine shop for rapid prototyping. The parts were built up in an identical configuration and of the same material. The rapid prototype machine traced out an airfoil cross-section and then continued to build up material in the spanwise direction, cross-section by cross-section. Thus, the final parts had identical surface properties, but slight ridges running in the chordwise direction where each deposited layer met the next. After fabrication, a threaded rod was attached to each so the airfoils could be installed in the wind tunnel. The pictures of the final fabricated airfoils are shown in Figure 14.

Figure 14. Fabricated RP airfoils: a) Continuous morphed profile, b) Discontinuous flap.

The airfoils were tested by cycling through the support angles and measuring lift and drag forces. Six individual cycles were run and the results were averaged to form the plots below. The error bars correspond to a 95% confidence interval and were calculated using the AIAA standard, which combines random error with bias error [31]. The sources of bias error and the values are listed in Table 1. The plots are presented as function of support angle, which can be considered as the overall airplane angle of attack.

Table 1. Table of significant sources of bias error in wind tunnel testing [32].

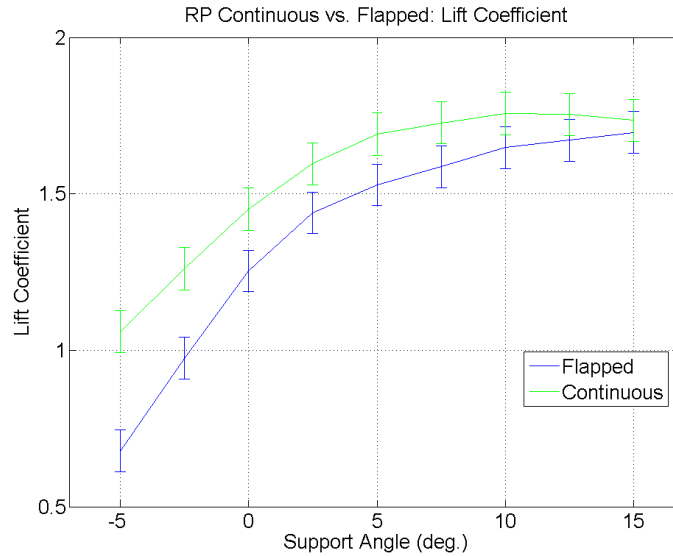| Device	Bias Value
Pressure Transducers	3.32 Pa
Load cells	0.068 N

Figure 15. Plot of coefficient of lift as a function of angle of attack

As Figure 15 shows, the continuous morphed airfoil shows significant improvement in lift coefficient compared to a flapped airfoil. At a support angle of -5 deg., the lift coefficient improvement with continuous is 0.38 while at 5 deg. the improvement is 0.11. The improvement decreases slightly with support angle. Towards the higher support angle the airfoils reach their maximum lift coefficient and then begin to stall, which is why the two lift curves appear to converge at these higher support angles.
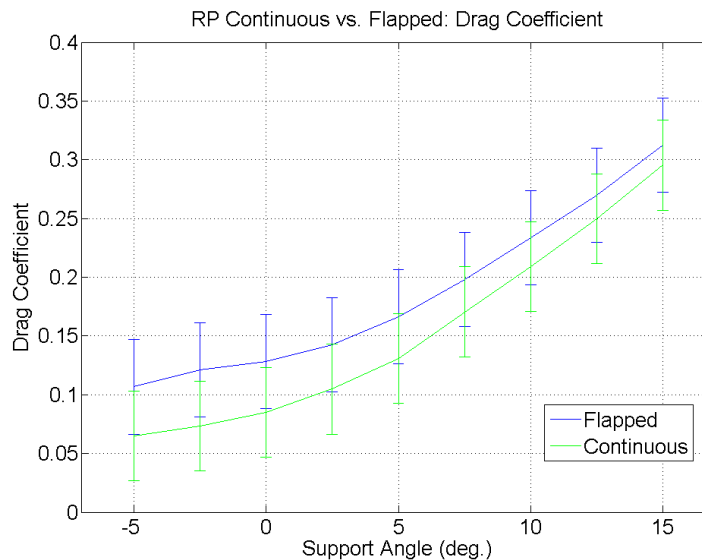

Figure 16. Plot of drag coefficient as a function of support angle for both flapped and continuous airfoils.

As Figure 16 illustrates, the drag is higher for the flapped airfoil compared to the continuous airfoil, as might be expected for a discontinuous flapped geometry that would be prone to flow separation. As support angle increases the difference between the two airfoils decreases. Again this is likely due to separation effects as the airfoil nears stall. The error bars are relatively large due to the low values of drag force measured by the load cells, but the trend of the morphed geometry is consistently less than the flapped airfoil. The relatively large drag measurements relative to the initial tests is likely due to the ridged surface texture that is inherent to the rapid prototyping process. The important point is that the geometry and surface texture was identical between bother specimens, and should be

fully comparable to determine the effects of the geometries alone, thus strengthening the implication that the morphed airfoil geometry is a lower drag solution.
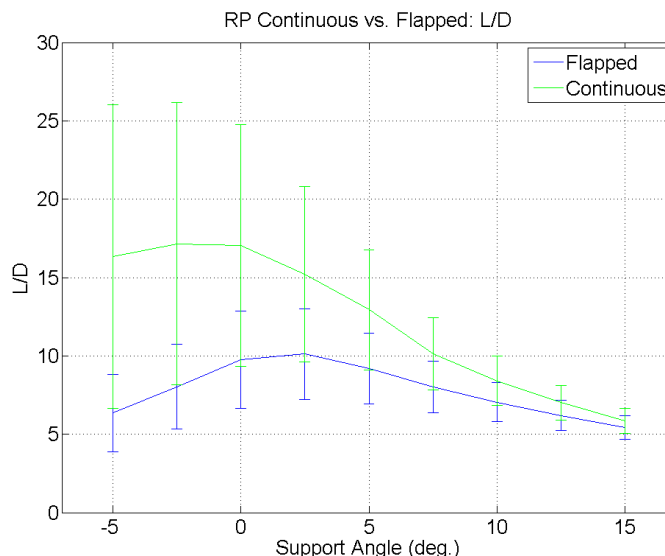

Figure 17. Plot of the lift to drag ratio as a function of support angle for both flapped and continuous airfoils.

In looking at the lift-to-drag ratio in Figure 17, the data suggests that the continuous airfoil has a significant improvement in L/D compared to the flapped airfoil. However, the error bars are significant, particularly at low support angles. The continuous airfoil data in particular has a large error at low support angles. This larger error is a result of the lower drag. Drag is lowest in the continuous airfoil at low support angles and the low value means that the bias error represents a larger percentage of the overall signal. Thus, when propagated to the calculation of L/D the error becomes quite significant. Even despite this large error, there is evidence that a continuous airfoil offers a larger L/D compared to a flapped airfoil.

The wind tunnel tests have shown a significant increase in lift with the continuous airfoil. The continuous airfoil also has slightly less drag. These effects combine to produce a larger L/D ratio. This is consistent with theory, as a continuous airfoil should be more aerodynamically streamlined than a flapped airfoil given that the only difference is continuity in airfoil geometry. However, the large error in drag and correspondingly in L/D ratio mean there is some uncertainty in the conclusions.

B. Size

Size of control actuators can be a significant design consideration depending on the scale of the air vehicle in question, and particularly for MAVs where space is at a minimum. From a packaging standpoint, the conformal MFC actuators (which are 0.012" thick) require virtually no volume, because they are embedded in the aircraft skins. This is a distinct advantage over servomotor actuators. However, they require an additional drive circuit to supply the high voltage inputs and control the morphing deflections, which must be considered from a system-level view. A custom high-voltage amplifier board was designed and fabricated for the current research effort in collaboration with AM Power Systems. The final driver board measured 2.2" x 3.4" x 0.5", and weighed roughly 0.071 lb (32 grams). Compare that with the servo measurements of 1.25" x 0.43" x 1.13", with multiple servos used in the vehicle design. The high voltage drive circuit is capable of controlling both the aileron and elevator channels for vehicle flight control, replacing two to three servo actuators. In contrast to servos with direct mechanical linkages that constrain actuator alignment and placement, this circuit board can be independently placed within the fuselage to strategically locate the volume and weight to favorably adjust the center of gravity.

C. Weight

Weight is a critical driving parameter in most air vehicle designs. Morphing aircraft structures have been hampered from broader use in air vehicle production for a variety of reasons, but one of the more prominent concerns is the potential weight increase of additional structure or electronic components. The morphing structures and electronic drive circuitry for this effort were designed with minimizing weight as a clear objective. Servo

actuators are a mature technology and widely used in the MAV and UAV markets, and therefore they set the bar for weight goals of morphing systems. A list of all of the components used in the servo based aileron system and the morphing aileron system are shown in Table 2 for comparison.

Table 2. Weight comparison of morphing and servomotor aileron systems.

Servo-Actuated Ailerons		Morphing Ailerons (3 MFC Bimorphs per Side)		Morphing Ailerons (2 MFC Bimorphs per Side)	
Item	**Weight (g)**	**Item**	**Weight (g)**	**Item**	**Weight (g)**
Servo Mount	2.1	Power Supply Mount	2.1	Power Supply Mount	2.1
Servo with Arm and Wire	9.3	High Voltage Power Supply (1/2 of total)	16.0	High Voltage Power Supply (1/2 of total)	16.0
Ball link assembly	2.6	Inboard Connectors	0.8	Inboard Connectors	0.8
Flex Cable	2.6	Wire	4.1	Wire	4.1
Clevis	1.2	Outboard Connectors	3.0	Outboard Connectors	3.0
Control Horn	1.0	Removed Wing Sections	-24.3	Removed Wing Sections	-24.3
Plastic hinges	1.2	MFC Aileron Patches	33.4	MFC Aileron Patches	28.1
		Wiper	4.5	Wiper	4.5
Total Weight (g)	**20.0**		**39.6**		**34.3**
% 1 Servo Baseline	**100%**		**198%**		**172%**
% 2 Servo System	**100%**		**118%**		**102%**

The servo and morphing systems were both minimized in weight to make this fair comparison. As can be seen from the tabulated data, the morphing systems weigh more than the servo-actuated aileron implementation. The largest weight contributor for the servo system is the servo actuator itself. For the morphing system, the MFC actuators are the primary weight source, with the drive electronics being the other key contributor. The elimination of existing composite structure is significant, and demonstrates that the MFC actuators are functioning as the significant structural member of the control surface. There are options as to how many servos are employed and how many MFCs are used to actuate the morphing. For the extreme case of a single servo versus the morphing case with three bimorphs per aileron patch, the morphing system is almost double the weight. Reducing the morphing actuation level to two MFC bimorphs results in a weight difference of 72%. If two servos were used to increase actuation power or provide some level of redundancy, the weight differences are not as severe. The lightest morphing configuration (2 bimorphs per side) is only 2% heavier than the servo configuration employing two servo actuators. As can be seen, there are trades that can be made in control power and redundancy that make the morphing system comparable in weight.

In a second case, observe the weight breakdown for the horizontal tail and elevator actuation system, as seen in Table 3.

Table 3. Weight comparison of morphing and servomotor elevator systems.

Servo-Actuated Elevator		Morphing Elevator (2 MFC Bimorphs)	
Item	**Weight (g)**	**Item**	**Weight (g)**
Servo Mount	1.9	Power Supply Mount	2.1
Servo with Arm and Wire	9.3	High Voltage Power Supply (1/2 of total)	16.7
EZ link	1.0	Forward Connectors	0.4
Pushrod and housing	4.7	Wire	2.0
Clevis	0.6	Aft Connectors	1.5
Control Horn	0.5	MFC Elevator Actuators	7.7
Non-morphing composite structure	18.9	Morphing Elevator composite structure	8.1
Plastic hinges	0.6		
Total Weight (g)	**37.5**		**38.5**
% Servo Baseline	**100%**		**103%**

In the data presented in Table 3, one can see that the overall weight is very similar. The morphing system is only 3% heavier than the servo-based elevator/tail system, but the differences are in the detailed component breakdown. In this comparison, the largest weight contributor for the servo-actuated system is the composite structure of the tail and flap, with the servo being the next heaviest item. The composite structure used in the morphing design weighs less than that used in the servo design because the MFC actuators are functioning as a load-bearing member of the structure. The elevator design incorporates only two MFC bimorphs, and therefore the actuator weight is reduced compared to the aileron. The electronics weight for the morphing system is the largest contributor, pointing out the multidisciplinary nature of this design problem to minimize weight.

In the two weight comparisons, it can be seen that the morphing system is in general heavier, but still comparable to the servo-actuated system. If there are other areas where the morphing flight control actuation is superior, this manageable penalty in weight could be justified for certain applications.

D. Power

An experimental study was performed to assess the power draw of both systems. While the MFC actuators are capacitive in nature, and only require electric current when charging or discharging, the high voltage electronics to supply these inputs require a certain amount of idle power. The power draw of the drive circuitry is reported here, rather than the power into and out of the MFC actuator, and therefore includes the efficiency of the power electronics. The power draw of the digital servomotor was calculated from voltage and current measurements sampling at 20 kHz to accurately capture the pulses of current supplied to the digitally controlled motor. The instantaneous power was calculated from the voltage and current measurements for each actuation technology. The average power draw and peak power draw are shown for a range of frequencies in Figure 18.
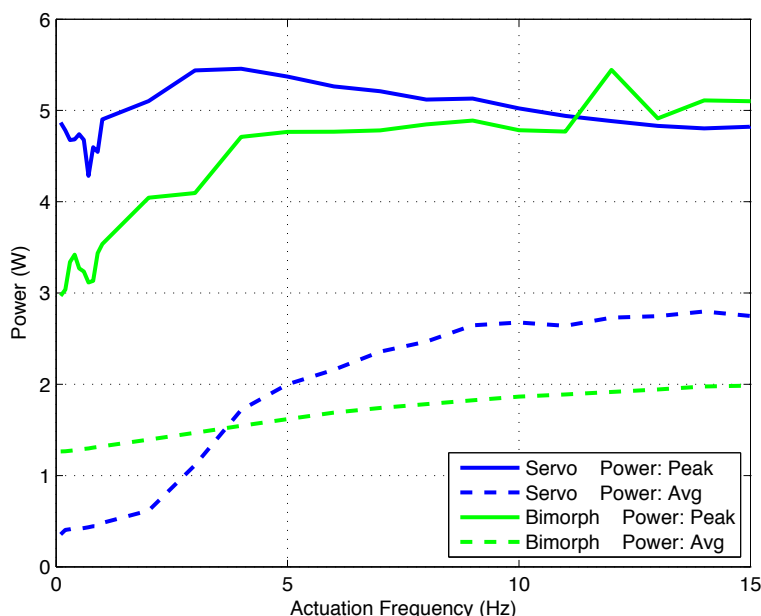

Figure 18. Comparison of the servo and bimorph airfoil power draw for the unloaded condition.

The peak power for the MFC morphing is generally less than or equal to that of the motor, and the average power is lower for higher frequency actuation. The drive circuitry for the MFC morphing actuation was designed with minimizing size and weight as the main objective, and could be further optimized to be more power efficient. The conclusion is that the morphing system power consumption is comparable to a micro servo actuator and superior in certain cases, with the potential for further improvement.

When the servo actuator is loaded (resisting a torque) the current draw rises and the power increases to hold the desired angular command. The MFC morphing technology is purely actuated through voltage level, and its power is not affected by loading, rather its deflection is affected. Care must be taken to design the morphing structure to perform well under load to fully take advantage of this benefit in power consumption.

E. Actuation Bandwidth

Actuator control bandwidth is a key parameter in MAV and UAV flight control applications, and could be critical for operations in urban environments or for agile maneuvers. A comparison between the MFC morphing and servo actuated airfoils is shown in Figure 19. The frequency response test data, presented as a Bode plot, was fitted with a curve in order to provide a smooth representation in which to compare the gain (magnitude of response compared to reference signal) and phase angle (lag behind reference signal).
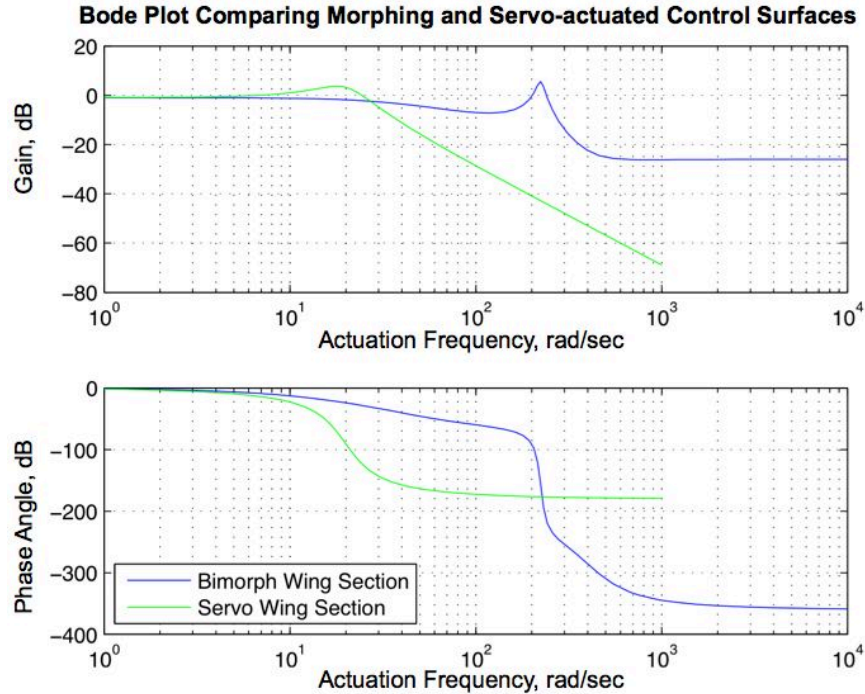

Figure 19. Bandwidth comparison of morphing actuation and servomotor actuation, showing an order of magnitude benefit for the case analyzed (31 Hz vs. 3 Hz).

Figure 19 shows that the morphing flight control actuation attains a bandwidth of roughly 30 Hz (resonance at 31 Hz), while the servo is limited to 3 Hz before attenuation of the response ensues. This order of magnitude increase in control bandwidth is significant and could be an enabling technology in MAV and UAV designs. It should be noted that the morphing bandwidth was limited by the structural dynamics of the flexible composite structure, which was designed for maximum deflection and low dynamic pressure aerodynamics. For stiffer structures, morphing actuation would likely be able to reach bandwidth values of 100 Hz or faster. The data clearly show that the MFC piezoelectric-based morphing is superior from a speed/bandwidth standpoint.

F. Reliability

Testing to assess the reliability of MFC actuators in a morphing structure is ongoing. These tests involve cycling an MFC test specimen for 10^6 cycles or until MFC failure, while measuring MFC performance periodically. The MFC bimorph specimen has been cycled 100,000 times (10^5) going from -100% to +100% actuation, without electrical shorting or structural failure. The deflection and frequency response of the specimen were recorded at 10,000, 20,000, 30,000, 40,000, 50,000 and 100,000 cycles. Figure 20 shows the deflection extents during all tests. Figure 21 shows the initial frequency response collected at 10,000 cycles to the frequency response at 50,000 cycles.
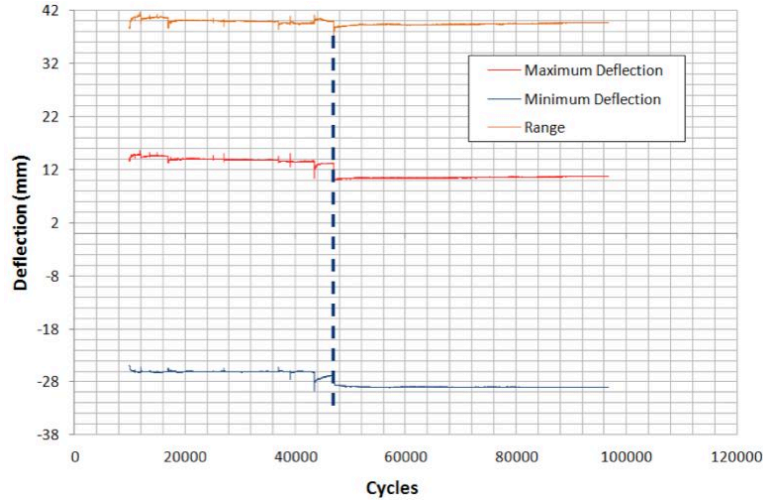
American Institute of Aeronautics and Astronautics

Figure 20. MFC deflection during cycle testing.

No significant degradation in MFC output has been observed over the 10^5 cycles performed to date. The discontinuities in the deflection history are mainly due to start-up transients between tests performed on different days and could be a result of slight changes in the experimental setup. The dotted line in Figure 20 represents when the reliability specimen was removed from and returned to the experimental setup, and then 50,000 continuous cycles were performed. During those 50,000 cycles no appreciable change was observed in output. While the bias in measurement of the deflections may have changed from day to day, the overall range of output deflection stayed roughly constant at 41 mm, implying no degradation in output over this period. Figure 21 demonstrates that the frequency response after 50,000 cycles was virtually identical to the initial data collected at 10,000 cycles.
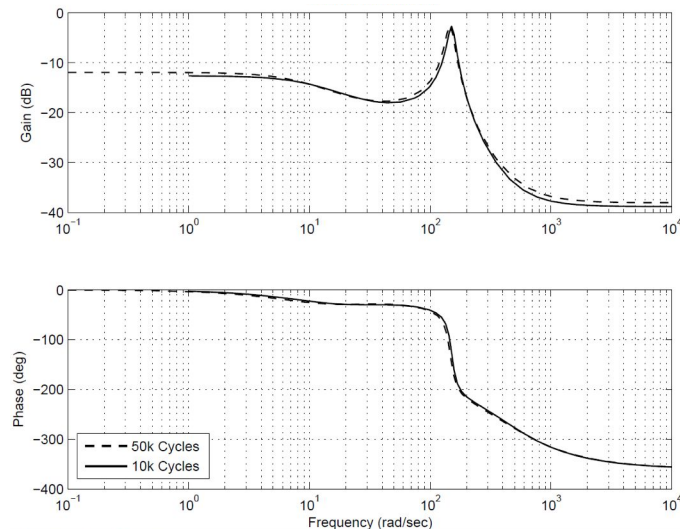

Figure 21. Bandwidth comparison during cycle testing.

While the reliability testing has not been fully completed, the initial results show promise and feasibility of using MFC morphing actuation in UAV and MAV applications. Cycle testing of the servo system has not yet been completed; therefore, a quantitative comparison cannot be shown. However, conceptually the presence of internal gears, external linkages and hinges that can jam or get clogged with sand do pose a potential reliability issue.

VI. Future Work

Flight tests of two vehicles, one incorporating the morphing actuation and the other using servo-actuation, will be executed in the coming months. The onboard data collection of vehicle states will be a primary metric for evaluating the performance of each vehicle in executing controlled maneuvers. Response speed, minimum turn

American Institute of Aeronautics and Astronautics

radius, and response to control surface doublets will be evaluated. Reliability tests of the morphing actuator to 10^6 cycles needs to be completed, in addition to testing the reliability of the servo actuator to compare with the results for the MFC actuators. Additional 3-dimensional wind tunnel tests in the future could also be used to precisely measure the control effectiveness of each approach.

VII. Conclusions

The effort to develop and compare MFC-based morphing control actuation to traditional servo-linkage implementations has yielded several conclusions. Aerodynamically, the conformal shape changes result in more efficient control force generation demonstrated by higher lift and superior lift-to-drag ratios. The MFC actuators require virtually no volume for integration, but the drive electronics must be considered from a size, weight and power standpoint. The volume of the MFC drive electronics can be independently located from the actuators, allowing more freedom in layout of the vehicle and center of gravity placement. While the morphing implementation weighs slightly more than the servo-linkage implementation, the weight is comparable and not necessarily prohibitive. The average power consumption for morphing actuation is comparable to servo-actuation and is lower for high frequency actuation. The peak power draw of the servos exceeded that of the morphing actuation for almost all cases. The bandwidth of the MFC morphing control surface was an order of magnitude higher than the servo-actuated control surface. The bandwidth of the morphing flight control actuation as tested was limited by the natural frequency of the structure, but could be further increased if the natural frequency was tailored for high frequency actuation. Reliability testing has shown no failures or loss of performance over 10^5 cycles, and the sealed, solid-state nature of the MFC morphing actuators eliminates linkages, hinges, and moving parts, thereby potentially increasing overall system reliability.

Acknowledgments

References

[1] Williams, R. B., "Nonlinear Mechanical and Actuation Characterization of Piezoceramic Fiber Composites," Ph.D. Dissertation, Mechanical Engineering Dept., Virginia Tech, Blacksburg, VA, March 22nd, 2004.

[2] Sodano, H., Park, G., and Inman, D., "The Use of Macro-Fiber Composites in Structural Vibration Applications," Mechanical Systems and Signal Processing, 2003.

[3] Stewart, K., J. Wagener, G. Abate, M. Salichon, "Design of the Air Force Research Laboratory Micro Aerial Vehicle Research Configuration", AIAA Paper 2007-667, 45th Aerospace Sciences Meeting and Exhibit, Reno, NV, 8-11 January, 2007.

[4] Stewart, K., K. Blackburn, J. Wagener, J. Czabaranek, G. Abate, "Development and Initial Flight Tests of a Single-Jointed Articulated-Wing Micro Air Vehicle", AIAA Paper 2008-6708, AIAA Atmospheric Flight Mechanics Conference, Honolulu, HI, 18-21 August, 2008.

[5] Lind, R., M. Abdulrahim, K. Boothe and P. Ifju, "Morphing for Flight Control of Micro Air Vehicles", European Micro Air Vehicle Conference, Braunschweig, Germany, July 2004.

[6] Amprikidis M. and J. E. Cooper, "Development of Smart Spars for Active Aeroelastic Structures", AIAA Structures, Structural Dynamics and Materials Conference, AIAA-2003-1799, 2003.

[7] Shkarayev, S. W. Null, and M. Wagner, "Development of Micro Air Vehicle Technology with In-Flight Adaptive-Wing Structure" NASA CR-2004-213271, 2004.

[8] Gad-el-Hak, M., "Micro Air Vehicles: Can They be Controlled Better?," Journal of Aircraft, Vol. 38, No. 3, p. 419 – 429, 2001.

[9] Stanford, B., Abdulrahim, M., Lind, R., and Ifju, P., "Investigation of Membrane Actuation for Roll Control of a Micro Air Vehicle," Journal of Aircraft, Vol. 44, No. 3, p. 741 – 749, 2007.

[10] Garcia, H., Abdulrahim, M., and Lind, R., "Roll Control for a Micro Air Vehicle Using Active Wing Morphing," AIAA Guidance, Navigation, and Control Conference and Exhibit, Austin, TX, AIAA-2003-5347, 2003.

[11] Heryawan, Y., Park, H., Goo, N., Yoon, K. and Byun, Y., "Structural Design, Manufacturing, and Wind Tunnel Test of a Small Expandable Wing," Key Engineering Materials, Vol. 306 – 308, pp. 1157 – 1162, 2006.

[12] Bilgen, O., Kochersberger, K., Diggs, E., Kurdila, A., Inman, D., "Morphing Wing Aerodynamic Control via Macro-Fiber-Composite Actuators in an Unmanned Aircraft," AIAA Paper 2007-2741, AIAA InfoTech@Aerospace Conference, Rohnert Park, CA, May, 2007.

[13] Bilgen, O., Kochersberger, K., Diggs, E. C., Kurdila, A. J., & Inman, D. J., "Morphing Wing Micro-Air-Vehicles via Macro-Fiber-Composite Actuators," 48th AIAA/ASME/ASCE/AHS/ASC Structures, Structural Dynamics, and Materials Conference, Honolulu, HI, April 23 – 26, 2007.

[14] Lee, C., Hong, G., Ha, Q., and Mallinson, S., "A Piezoelectrically actuated micro synthetic jet for active flow control," Science Direct Series, Elsevier, Vol. 108, pp. 168 – 174, 2003.

[15] Ghee, T., and Leishman, G., "Effects of Unsteady Blowing on the Lift of a Circulation Controlled Cylinder, Journal of the American Helicopter Society, Vol. 35, No. 3, p. 90 – 93, 1990.

[16] Pern, N. J., Jacob, J., and LeBeau, R., "Characterization of Zero Mass Flux Flow Control for Separation Control of an Adaptive Airfoil," 3rd AIAA Flow Control Conference, San Francisco, CA, June 2006.

[17] Gern, F. H., Inman, D. J., & Kapania, R. K., "Structural and Aeroelastic Modeling of General Planform Wings with Morphing Airfoils," AIAA Journal, Vol. 40, No. 4, pp. 628-637, 2002.

[18] Marques, M., Gamboa, P., & Andrade, E., "Design of a Variable Camber Flap for Minimum Drag and Improved Energy Efficiency," AIAA/ASME/ASCE/AHS/ASC Structures, Structural Dynamics, and Materials Conference, Palm Springs, CA, May 4-7, 2009.

[19] Abdullah, E. J., Bil, C., & Watkins, S., "Application of Smart Materials for Adaptive Airfoil Control," AIAA Aerospace Sciences Meeting, Orlando, FL, January 5-8, 2009.

[20] Martin, T., Guitton, A., Schmit, R., & Glauser, M. N., "Development of a Morphing Micro Air Vehicle Wing Using The Combined POD and LSE Technique," AIAA Infotech@Aerospace, Arlington, VA, September 26-29, 2005.

[21] Ameri, N., Livne, E., Lowenberg, M. H., & Friswell, M. I., "Modeling Continuously Morphing Aircraft for Flight Control," AIAA Guidance, Navigation and Control Conference, Honolulu, HI, August 18-21, 2008.

[22] Lampton, A., Niksch, A., & Valasek, J., "Morphing Airfoils with Four Morphing Parameters," AIAA Guidance, Navigation and Control Conference, Honolulu, HI, August 18-21, 2008.

[23] Abdulrahim, M., Garcia, H., Ivey, G. F., & Lind, R., "Flight Testing a Micro Air Vehicle Using Morphing for Aeroservoelastic Control," AIAA/ASME/ASCE/AHS/ASC Structures, Structural Dynamics & Materials Conference, Palm Springs, CA, April 19-12, 2004.

[24] Bilgen, O., K. Kochersberger, D. Inman, O. Ohanian, "Novel, Bidirectional, Variable-Camber Airfoil via Macro-Fiber Composite Actuators", *Journal of Aircraft*, Vol. 47, No. 1, 2010.

[25] Bilgen, O., K. Kochersberger, D. Inman, O. J. Ohanian, "Macro-Fiber Composite actuated simply supported thin airfoils", Smart Materials and Structures, Vol. 19, 2010.

[26] Ohanian, O. J., E. Karni, C. Olien, E. Gustafson, K. Kochersberger, P. Gelhausen, B. Brown, "Piezoelectric Composite Morphing Control Surfaces for Unmanned Aerial Vehicles", SPIE Paper 7981-203, Proceedings of SPIE Smart Structures Conference, San Diego, CA, March 7-10, 2011.

[27] Probst, T., Kochersberger, K., Stiltner, B., Hickling, C., Ohanian, O., Karni, E., Olien, C., Blain, A., "Smart material actuators as a means of UAV flight control", AIAA Paper 2012-486, 50th AIAA Aerospace Sciences Meeting including the New Horizons Forum and Aerospace Exposition, Nashville, Tennessee, Jan. 9-12, 2012.

[28] Selig, M., "UIUC Airfoil Data Site," http://www.ae.uiuc.edu/m-selig/ads.html, (accessed July 20, 2009).

[29] Drela, M., Youngren, H., "XFOIL", http://web.mit.edu/drela/Public/web/xfoil/, (accessed January 5, 2011).

[30] Bilgen, O., *Aerodynamic and Electromechanical Design, Modeling, and Implementation of Piezocomposite Airfoils*, Ph.D. dissertation, Virginia Polytechnic Institute and State University, 2010.

[31] American Institute of Astronautics and Aeronautics, Assessment of Experimental Uncertainty with Application to Wind Tunnel Testing, 1999.

[32] Gustafson, E. Design, Simulation, and Wind Tunnel Verification of a Morphing Airfoil. Master's thesis. Virginia Polytechnic Institute and State University, 2011.